EDGE ARTICLE

Check for updates

Dithienonaphthobisthiadiazole synthesized by thienannulation of electron-deficient rings: an acceptor building unit for high-performance π-conjugated polymers†

Tsubasa Mikie, [ID] *[ab] Tomokazu Morioku,[a] Shota Suruga,[a] Momoka Hada, [ID] [b] Yuki Sato,[c] Hideo Ohkita [ID] [c] and Itaru Osaka [ID] *[ab]

The development of building units for π-conjugated polymers is a driving force in advancing the field of organic electronics. In this study, we designed and synthesized dithienonaphthobisthiadiazole (TNT) as a thiophene-fused acceptor (A) building unit and two TNT-based π-conjugated polymers named **PTNT2T** and **PTNT1-F**. We found that the microwave-assisted thiophene annulation reaction (thienannulation) of arylethynylated naphthobisthiadiazole (NTz) *via* C−H functionalization effectively produced TNT moieties. With the π-extended structure of TNT, the polymers had rigid backbones that benefited in-plane and out-of-plane charge carrier transport. Organic field-effect transistors (OFETs) based on **PTNT2T** exhibited hole mobilities as high as 1.10 cm^2 V^{-1} s^{-1}. Furthermore, organic photovoltaic cells (OPVs) based on **PTNT1-F** showed high power conversion efficiencies of up to 17.4% when combined with a nonfullerene acceptor. This work provides an efficient method for the thienannulation of electron-deficient rings to access thiophene-fused A building units and shows the great promise of TNT as a building unit for high-performance π-conjugated polymers for organic electronic devices.

Introduction

π-Conjugated polymers are an important class of materials in organic electronics.[1] This is evidenced by their broad applications in organic field-effect transistors (OFETs),[2,3] organic electrochemical transistors (OECTs),[4,5] organic photovoltaics (OPVs),[6–9] organic photodetectors (OPDs),[10] and organic thermoelectrics (OTEs).[11] A driving force in advancing this research field is the development of π-conjugated polymers with alternating donor (D)–acceptor (A) building units, that is, D–A polymers.[12,13] For instance, they can have small bandgaps owing to the intrachain D–A interaction, which is beneficial for near-IR absorption and thereby OPVs and OPDs.[14] In addition, they can form a crystalline structure with close π–π stacking owing to the interchain dipole–dipole interaction, which is beneficial for charge carrier transport.[12] Through the judicious choice of the D and A building

units, the electronic, optical, and packing structure of the polymers can be precisely controlled to match the needs of the application. Thus, the design of building units is a key issue in the development of D–A polymers. A promising design strategy for the building unit is the fusion of thiophene rings to the end of a heterocyclic structure, which can enhance the backbone rigidity and interchain interaction due to the π-extended structure.[15]

A number of thiophene-fused rings as the D building unit, such as thienothiophene (TT),[16] benzodithiophene (BDT),[17] naphthodithiophene (NDT),[18,19] cyclopentadithiophene (CDT),[20,21] and indacenodithiophene (IDT)[22–24] (Fig. 1a), have been investigated for the development of π-conjugated polymers in organic electronics. Key to the synthesis of thiophene-fused rings is the thiophene annulation reaction (thienannulation). TT, BDT, and NDT are typically synthesized *via* thienannulation.[25] On the other hand, thiophene-fused rings as A building units are limited to such imide- and amide-containing compounds as dithienophthalimide (DPI),[26,27] naphthodithiophenebisimide (NDTI),[28] dithienylthiophenebisimide (TBI),[29,30] and thienoisoindigo (TIID)[31,32] (Fig. 1b). An example of a nonimide or nonamide thiophene-fused A building unit is dithienobenzothiadiazole (DTBT) (Fig. 1c),[33] in which two thiophenes are fused to the end of benzothiadiazole, a well-known A building unit.[34] A DTBT-based polymer, D18, exhibits high power conversion efficiencies (PCEs) approaching 20% in

[a]Applied Chemistry Program, Graduate School of Advanced Science and Engineering, Hiroshima University, 1-4-1 Kagamiyama, Higashi-Hiroshima, Hiroshima 739-8527, Japan

[b]School of Engineering, Hiroshima University, 1-4-1 Kagamiyama, Higashi-Hiroshima, Hiroshima 739-8527, Japan

[c]Department of Polymer Chemistry, Graduate School of Engineering, Kyoto University, Kyoto 615-8510, Japan. E-mail: mikie@hiroshima-u.ac.jp; iosaka@hiroshima-u.ac.jp

† Electronic supplementary information (ESI) available. See DOI: https://doi.org/10.1039/d4sc05793g
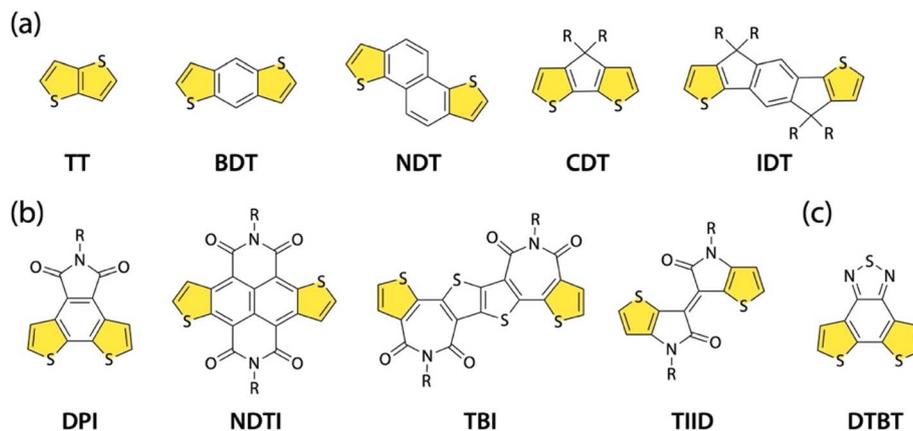
Fig. 1 Chemical structures of thiophene-fused rings (a) as the D building unit: TT, BDT, NDT, CDT, and IDT; (b) as the A building unit based on imide or amide compounds: DPI, NDTI, TBI, and TIID; and (c) as the A building unit based on the benzothiadiazole compound: DTBT.

nonfullerene (NFA) OPVs.[35,36] One possible reason for the limited number of thiophene-fused A building units is the difficulty of applying conventional thienannulation to the A units. Among those thiophene-fused A building units, only NDTI was synthesized using thienannulation. Therefore, in addition to the exploration of new thiophene-fused A building units, the development of a new thienannulation methodology applicable to A units is important for the creation of high-performance D–A polymers.

Naphtho[1,2-c:5,6-c′]bis[1,2,5]thiadiazole (NTz) (Fig. 2a), in which two benzothiadiazoles are fused, is a promising A building unit.[37–39] We previously reported that NTz-based polymers such as **PNTz4T** and **PNTz1-F** showed good performance in OFETs and/or OPVs (Fig. 2b).[40,41] Herein, as a new family of thiophene-fused A building units, we designed and synthesized dithieno[3′,2′:3,4; 3″,2″:7,8]naphtho[1,2-c:5,6-c′]bis([1,2,5]thiadiazole) (TNT) (Fig. 2a), in which thiophenes are fused to the ends of NTz. Notably, we found that with the assistance of microwaves in the thienannulation reaction via C–H functionalization reported by

Itami and co-workers,[42] arylethynylated NTz precursors were converted into TNT derivatives in reasonably high yields. The TNT-based monomers were homopolymerized and copolymerized with a BDT-based monomer, providing π-conjugated polymers **PTNT2T** and **PTNT1-F**, which are regarded as the counterparts of **PNTz4T** and **PNTz1-F**, respectively (Fig. 2d). To study the impact of thiophene fusion to the ends of NTz, we discuss the properties, thin film structures, charge carrier transport properties, and photovoltaic performances of **PTNT2T** and **PTNT1-F** in comparison with those of NTz counterparts **PNTz4T** and **PNTz1-F**.

Results and discussion

Synthesis of TNT derivatives via thienannulation

Key to constructing the TNT structure is the thienannulation of NTz via the arylethynylated NTz precursor (Scheme 1). The reaction can be partially regarded as the formation of benzothiophene. Conventional thienannulation reactions use
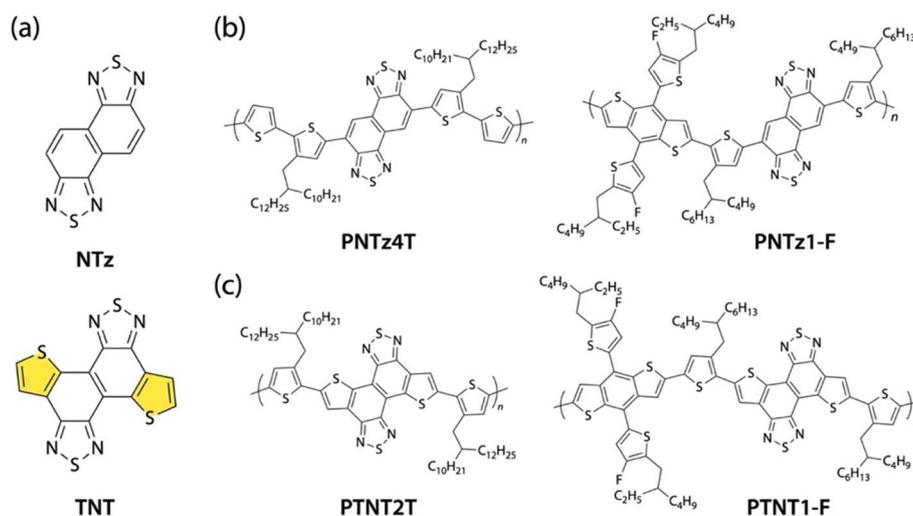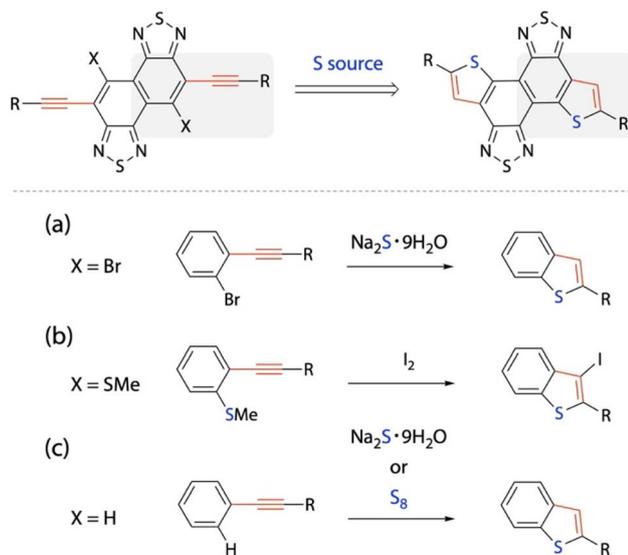

Fig. 2 Chemical structures of (a) naphtho[1,2-c:5,6-c′]bis[1,2,5]thiadiazole (NTz) and dithieno[3′,2′:3,4; 3″,2″:7,8]naphtho[1,2-c:5,6-c′]bis([1,2,5]thiadiazole) (TNT); (b) NTz-based polymers **PNTz4T** and **PNTz1-F**; and (c) TNT-based polymers **PTNT2T** and **PTNT1-F**.

Scheme 1 Synthetic strategy for the construction of thiophene rings at the ends of NTz. (a and b) Conventional thienannulations of disubstituted benzene and (c) thienannulations of monosubstituted (ethynylated) benzene *via* C–H functionalization.

precursors with a halogen or an alkylthio group at the *ortho* position of the arylethynyl group (Scheme 1a and b).[25,43] On the other hand, it has been reported that non-*ortho*-substituted arylethynylbenzene moieties undergo thienannulation with the use of sodium sulfide hydrate ($Na_2S \cdot 9H_2O$)[28] or elemental sulfur (S_8)[42] to form benzothiophene moieties (Scheme 1c). As these thienannulation reactions are simpler than the conventional ones for benzothiophene formation using arylethynylbenzene moieties, we exploited these synthetic protocols for the formation of the TNT structure.

Scheme 2 shows the synthetic route to TNT derivatives. To examine the thienannulation, we synthesized an ethynylalkylthiophene-flanking NTz derivative (**3**) using the Sonogashira cross-coupling reaction between dibromo-NTz (**1**) and 2-ethynyl-3-alkylthiophene (**2**), where R^1 = 2-decyltetradecyl (DT) and R^2 = H. It should be noted that the alkyl groups were attached to the 3-position of the thiophene ring to avoid the formation of a double-cyclized byproduct during the thienannulation when S_8 was used, such as thienothiophene-flanking NTz derivatives. We first

tested the thienannulation of **3** using $Na_2S \cdot 9H_2O$. It, however, provided a complex mixture without a TNT derivative (**4**). We then tested the thienannulation of **3** using S_8 (2 equivalents) following the reported protocol.[42] The use of DMF and DMAc as the solvent at 140 °C afforded **4**. In contrast, the use of NMP, DMSO, and DMPU did not afford **4** and likely led to decomposition at the same temperature (Table 1, entries 1–6). However, the yield was limited to 9% (DMAc) and remained so even when the temperature was increased to 180 °C. It has been proposed that this type of thienannulation is initiated by the electrophilic reaction of the substrate with S_8. In this regard, it is quite difficult for **3** to undergo an electrophilic reaction owing to the strong electron deficiency of NTz. We decided to use a microwave reactor to accelerate the reaction. As a result, the yield was improved to 16% (entry 7) and 25% when the amount of S_8 was increased to 4 equivalents (entry 8) (Table 1). We further hypothesized that the α-position of alkylthiophene could cause some side reactions and decrease the yield. Thus, we synthesized **3** using **2** with the *tert*-butyldimethylsilyl (TBS) group as R^2 (Scheme S1†). Notably, the thienannulation of silyl-protected **2** significantly improved the yield of **4** to 42% (Table 1, entry 9). Moreover, the gram-scale synthesis further improved the yield to 59%. It is worth noting that when the less bulky 2-hexyldecyl (HD), 2-butyloctyl (BO), and dodecyl (C12) groups were attached to **3**, the yield was further improved to 46–56% (entries 10–12). When we applied the optimized thienannulation conditions to the BTz derivative, alkylthiophene-flanking DTBT was obtained in a similar yield (50%) to the TNT derivative (Scheme S2†). This methodology was able to more easily access DTBT building units than the conventional methodology.[33]

Synthesis of TNT-based polymers

Considering the solubility of the polymer, we selected DT and HD groups as the alkyl groups for the synthesis and evaluation of **PTNT2T** and **PTNT1-F**, respectively. The desilylation of **4a** (R^1 = DT) and **4b** (R^1 = HD) quantitatively afforded **5a** and **5b**, and the subsequent dibromination yielded the TNT monomers (**6a** and **6b**) in approximately 90% (Scheme 3). Finally, **PTNT2T** and **PTNT1-F** were synthesized by the homopolymerization of **6a** (R^1 = DT) using hexamethylditin and the copolymerization of **6b** (R^1 = HD) with a distannylated benzodithiophene derivative (**7**), respectively, *via* the Stille cross-coupling reaction. The number-average molecular weight (M_n) and the dispersity ($Đ$) were 20
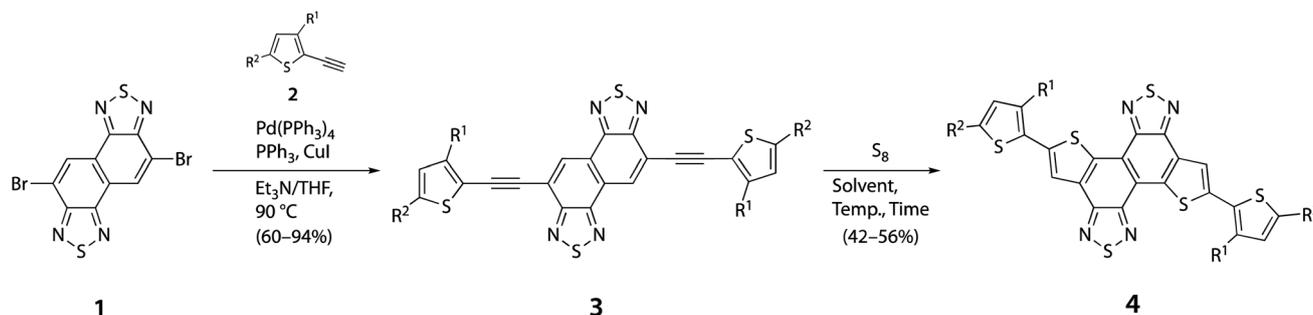
Scheme 2 Synthesis of TNT derivatives *via* thienannulation.

Table 1 Reaction conditions tested for the thienannulation of 3^a

| Entry	Substituent		Conditions				
	R^1	R^2	Solvent[b]	S_8 (equiv.)	Temp.[c] (°C)	Time	Yield (%)
1	DT	H	DMF	2	140	48 h	2
2	DT	H	NMP	2	140	48 h	n.d.
3	DT	H	DMSO	2	140	48 h	n.d.
4	DT	H	DMPU	2	140	48 h	n.d.
5	DT	H	DMAc	2	140	48 h	9
6	DT	H	DMAc	2	180	48 h	9
7	DT	H	DMAc	2	200 (microwave)	45 min	16
8	DT	H	DMAc	4	200 (microwave)	45 min	25
9	DT	TBS	DMAc	4	200 (microwave)	45 min	42 (59)[d]
10	HD	TBS	DMAc	4	200 (microwave)	45 min	46
11	BO	TBS	DMAc	4	200 (microwave)	45 min	50
12	C12	TBS	DMAc	4	200 (microwave)	45 min	56

[a] DT = 2-decyltetradecyl, HD = 2-hexyldecyl, BO = 2-butyloctyl, C12 = dodecyl, TBS = *tert*-butyldimethylsilyl. [b] DMF = *N,N*-dimethylformamide, NMP = *N*-methylpyrrolidone, DMSO = dimethyl sulfoxide, DMPU = *N,N'*-dimethylpropyleneurea, DMAc = *N,N*-dimethylacetamide. [c] Following the Arrhenius equation, the total amount of heat for microwave-assisted heating at 200 °C for 45 min is equivalent to that for heating at 140 °C for 48 h. [d] 1.5 g (1.1 mmol) of **3** was used.

000 and 2.0 for **PTNT2T**, and 41 000 and 2.1 for **PTNT1-F**, respectively (Fig. S1 and Table S1†). Interestingly, **PTNT2T** exhibited similar solubility to **PNTz4T** even though TNT was a more π-extended building unit than NTz. Both polymer solutions in chlorobenzene (CB) with a concentration of approximately 8 g L^{-1} remained in solution at room temperature after heating to 100 °C to dissolve the polymers. **PTNT1-F** showed similar solubility to **PNTz1-F** and was soluble in chloroform (CF) at around 40–50 °C when its molecular weight was similar to that of **PNTz1-F**. Thermogravimetric analysis revealed that both polymers were thermally stable up to 400 °C, and differential scanning calorimetry showed no phase transition peak below 350 °C (Fig. S2 and S3†).

Comparison of electronic properties between NTz and TNT

To examine the effect of thiophene-fusion on the electronic properties, we carried out the electrochemical and optical measurements for **5a** (**TNT2T**) in comparison with an NTz counterpart, **NTz4T** (Fig. 3a). Using cyclic voltammetry (CV), we determined the HOMO and LUMO energy levels (E_{HOMO} and E_{LUMO}, respectively), or ionization potential (IP) and electron affinity (EA), respectively, of the compounds (Fig. 3b). Based on the onset oxidation and reduction potentials (E_{ox} and E_{red}, respectively), the E_{HOMO} and E_{LUMO} of **NTz4T** were estimated to be −5.36 eV and −3.49 eV and those of **TNT2T** were −5.46 and −3.24 eV, respectively. Thus, the E_{HOMO} and E_{LUMO} of **TNT2T** were deeper and shallower by 0.10 and 0.25 eV than those of **NTz4T**, respectively. The lower E_{HOMO} of **TNT2T** than that of **NTz4T** is most likely due to the weaker electron-rich nature of the alkylthiophene moieties for **TNT2T** than the alkylbithiophene moieties for **NTz4T**. The shallower E_{LUMO} of **TNT2T** than that of **NTz4T** can be explained by the weaker electron-poor nature of the TNT moiety than the NTz moiety, because, in TNT, two electron-rich thiophenes are fused to NTz.
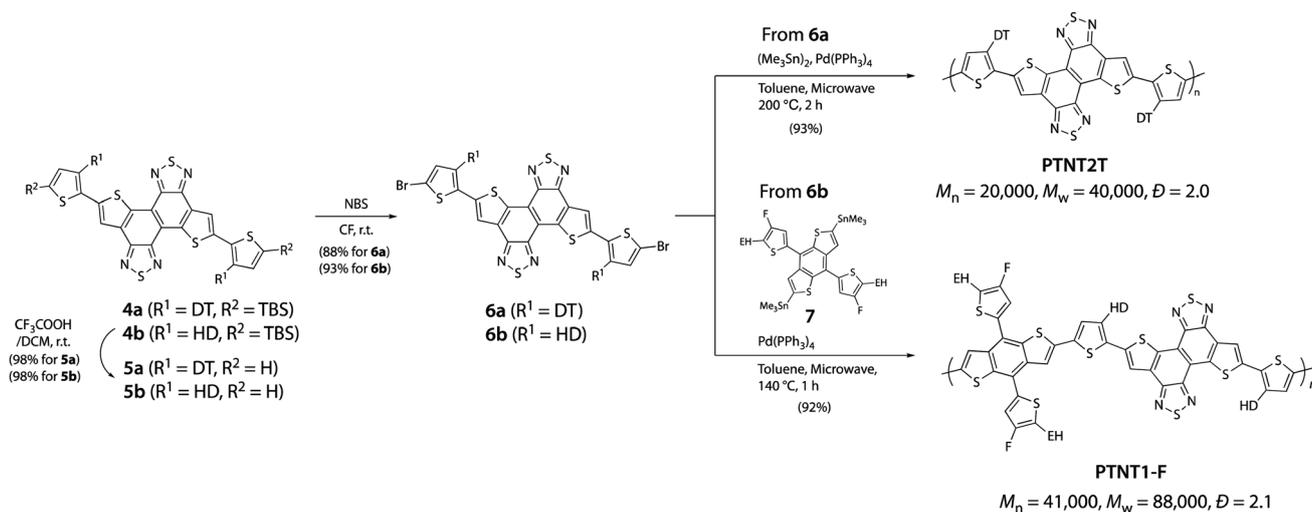
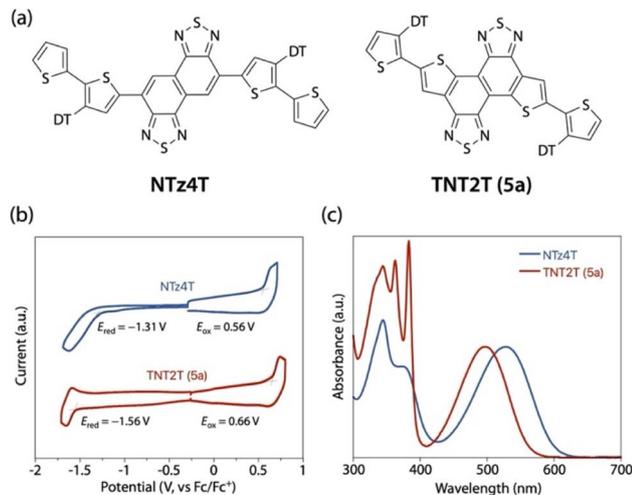**Scheme 3** Synthetic route to TNT-based polymers.

Fig. 3 (a) Chemical structures of **NTz4T** and **TNT2T** (**5a**) that correspond to the repeat unit for **PNTz4T** and **PTNT2T**. (b) Cyclic voltammograms and (c) UV-vis absorption spectra of **NTz4T** and **TNT2T** in solution.

Fig. 3c depicts the absorption spectra of the compounds in CB solution. The absorption band for **TNT2T** was blue-shifted by 30–40 nm compared to that for **NTz4T**; the absorption maxima (λ_{max}) and onset (λ_{onset}) for **NTz4T** were 528 nm and 600 nm and those for **TNT2T** were 497 nm and 561 nm, respectively. The blue-shift in **TNT2T** relative to that in **NTz4T** can be explained by the reduced intramolecular D–A interaction (push–pull effect); again, the alkylthiophene moieties as the D unit for **TNT2T** are less electron-rich than the alkylbithiophene moieties for **NTz4T**,

and the TNT moiety as the A unit for **TNT2T** is less electron-poor than the NTz moiety for **NTz4T**. These electronic properties are consistent with those predicted by the DFT calculation (Fig. S4†).

Polymer properties

The E_{HOMO} and E_{LUMO} of polymers were also evaluated by CV using the thin films (Fig. 4a). Based on the onset redox potentials, the E_{HOMO} and E_{LUMO} of **PTNT2T** were estimated to be −5.42 and −3.18 eV, respectively, which were deeper by 0.17 eV and shallower by 0.15 eV than those of **PNTz4T** ($E_{HOMO} = -5.25$, $E_{LUMO} = -3.33$ eV), respectively (Table 2). The E_{HOMO} and E_{LUMO} of **PTNT1-F** were estimated to be −5.53 and −3.17 eV, which were deeper by 0.15 eV and shallower by 0.14 eV than those of **PNTz1-F** ($E_{HOMO} = -5.38$ eV, $E_{LUMO} = -3.31$ eV), respectively.

The UV-vis absorption spectra of the polymers in the CB solution and the thin films are shown in Fig. 4b, and the corresponding parameters are summarized in Table 2. In solution, the λ_{max} and λ_{onset} for **PTNT2T** were 703 and 758 nm, respectively, which were blue-shifted by *ca.* 20 nm compared to those for **PNTz4T** ($\lambda_{max} = 717$ nm and $\lambda_{onset} = 784$ nm). **PTNT1-F** exhibited λ_{max} and λ_{onset} of 620 and 710 nm, which were significantly blue-shifted compared to those for **PNTz1-F** ($\lambda_{max} = 658$ nm and $\lambda_{onset} = 780$ nm). It should be noted that the main absorption bands in the thin films were similar to those in solution for each of the polymers, suggesting partial aggregation derived from the coplanar backbone. The λ_{max} and λ_{onset} in the thin film were similar to those in solution for all the polymers: **PTNT2T** ($\lambda_{max} = 705$ nm and $\lambda_{onset} = 777$ nm), **PNTz4T** ($\lambda_{max} = 720$ nm and $\lambda_{onset} = 800$ nm), **PNTz1-F** ($\lambda_{max} = 636$ nm and $\lambda_{onset} = 793$ nm), and
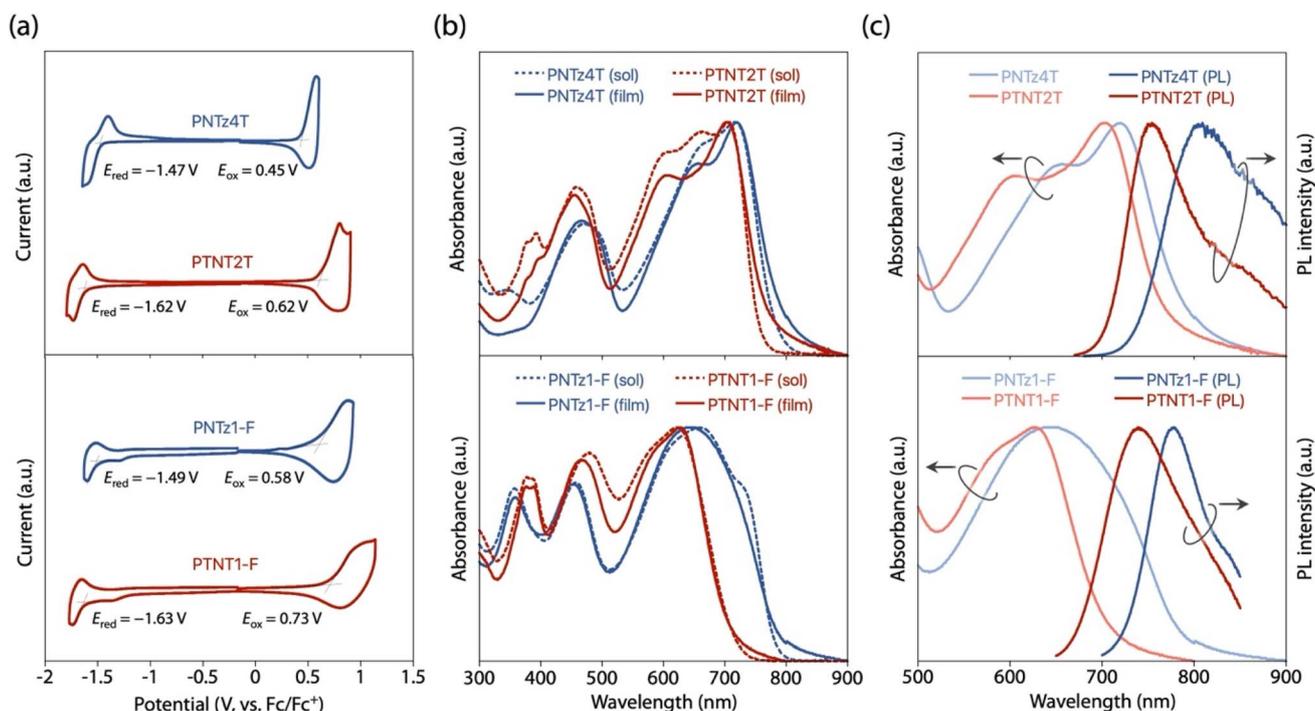

Fig. 4 (a) Cyclic voltammograms, (b) UV-vis absorption spectra in both solution and film, and (c) PL spectra along with UV-vis absorption spectra in film for **PNTz4T** and **PTNT2T** (upper panel), and **PNTz1-F** and **PTNT1-F** (lower panel).

Table 2 Electrochemical and optical properties of the polymers

Compounds	E_{HOMO}/IP^a (eV)	E_{LUMO}/EA^a (eV)	λ_{max}^b (nm)		λ_{onset}^c (nm)		$E_g^{opt\,d}$ (eV)	$\lambda_{max}^{em\,e}$ (nm)	ΔE_{SS}^f (eV)
			Sol	Film	Sol	Film			
NTz4T	−5.36	−3.49	528	—	600	—	—	—	—
TNT2T (5a)	−5.46	−3.24	497	—	561	—	—	—	—
PNTz4T	−5.25	−3.33	717	720	784	800	1.55	809	0.19
PTNT2T	−5.42	−3.18	703	705	758	777	1.60	754	0.11
PNTz1-F	−5.38	−3.31	658	636	780	793	1.56	778	0.36
PTNT1-F	−5.53	−3.17	620	629	710	711	1.74	739	0.29

^{a} Estimated using redox potentials determined from cyclic voltammograms. Solution samples were used for **NTz2T** and **TNT2T** and the thin film samples were used for the polymers. All the potentials were calibrated with the half-wave potential of the ferrocene/ferrocenium redox couple measured under identical conditions. HOMO and LUMO energy levels were estimated using the following equations, HOMO (eV): $-4.80 - E_{ox}^{onset}$, LUMO (eV): $-4.80 - E_{red}^{onset}$. ^{b} Absorption maximum. ^{c} Absorption onset. ^{d} Optical band gap calculated by using the following equation: E_g^{opt} (eV) $= 1240/\lambda_{edge}$ (nm). ^{e} Maximum emission excited at λ_{max}. ^{f} Stokes shift for polymer thin films in energy.

PTNT1-F (λ_{max} = 629 nm and λ_{onset} = 711 nm). Accordingly, the E_g^{opt} calculated from the λ_{onset} for **PTNT2T** was E_g^{opt} = 1.60 eV, wider than that for **PNTz4T** (E_g^{opt} = 1.55 eV). Similarly, **PTNT1-F** had a wider E_g^{opt} (1.74 eV) than **PNTz1-F** (E_g^{opt} = 1.56 eV). This agrees with the experimental result that the TNT-based polymers had deeper E_{HOMO} and shallower E_{LUMO} than the NTz-based polymers, as described above.

The variations in the energy levels and the absorption spectra between the NTz- and TNT-based polymers were similar to those observed between **NTz4T** and **TNT2T**. As discussed above, TNT is expected to have a weaker electron-poor nature than NTz, and hence the TNT-based polymers have reduced intrachain D–A interaction compared to the NTz-based polymers. This would result in larger E_g^{opt}s (blue-shifted absorption) and thus the shallower E_{LUMO}s and deeper E_{HOMO}s for the TNT-based polymers than for the NTz-based polymers. These polymer properties were consistent with the computation using the DFT method at the B3LYP/6-31g(d) level (Fig. S5†).

We also studied the PL spectra of the polymers in the thin film (Fig. 4c and Table 2). The emission maxima (λ_{max}^{em}) of

PTNT2T and **PNTz4T** were λ_{max}^{em} = 754 and 809 nm, respectively. Consequently, the Stokes shift value (ΔE_{SS}) for **PTNT2T** (ΔE_{SS} = 0.11 eV) was smaller than that for **PNTz4T** (ΔE_{SS} = 0.19 eV). Similarly, the λ_{max}^{em} of **PTNT1-F** and **PNTz1-F** were λ_{max}^{em} = 739 and 778 nm, respectively, and therefore, ΔE_{SS} for **PTNT1-F** (ΔE_{SS} = 0.29 eV) was smaller than that for **PNTz1-F** (ΔE_{SS} = 0.36 eV). These results suggest that the TNT-based polymers had higher backbone rigidity than their NTz-based counterparts, most likely due to the π-extended structure of TNT along the polymer backbone.

We further investigated the temperature dependence (20–100 °C) of the absorption spectra in the CB solution. In **PNTz4T** (Fig. 5a), the absorption spectrum largely blue-shifted and the absorption shape became featureless upon heating to 100 °C. By contrast, in **PTNT2T** (Fig. 5b), the absorption spectrum did not show such a large blue-shift and it still had vibronic structures
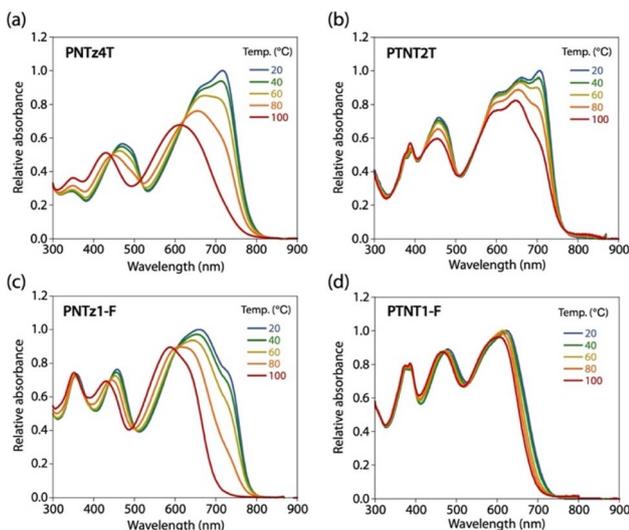

Fig. 5 Temperature-dependence of the absorption spectra in the CB solution for (a) PNTz4T, (b) PTNT2T, (c) PNTz1-F, and (d) PTNT1-F.

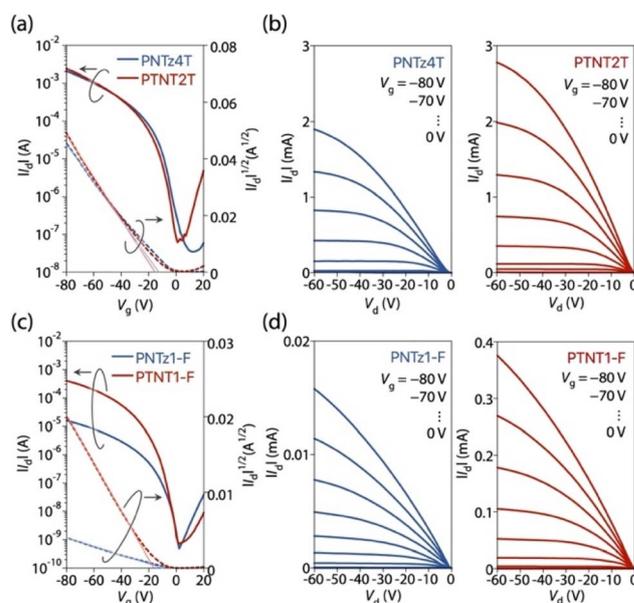**Fig. 6** (a and c) Transfer and (b and d) output curves of OFET devices: (a and b) PNTz4T and PTNT2T and (c and d) PNTz1-F and PTNT1-F.

Table 3 OFET and OPV properties

Polymer	OFET	OPV[b]			
	$\mu^{\text{FET}} [\mu_{\text{ave}}^{\text{FET}}]^{a}$ (cm^2 V^{-1} s^{-1})	$J_{\text{SC}} [J_{\text{SC}}^{\text{EQE}}]^{c}$ (mA cm^{-2})	V_{OC} (V)	FF	PCE [PCE$_{\text{ave}}$]^{d} (%)
PNTz4T	0.81 [0.65]	22.8 [22.9]	0.70	0.69	11.1 [10.8]
PTNT2T	1.10 [0.77]	22.5 [22.8]	0.80	0.74	13.4 [13.1]
PNTz1-F	0.004 [0.003]	24.5 [24.4]	0.79	0.69	13.3 [12.6]
PTNT1-F	0.18 [0.13]	27.1 [27.0]	0.86	0.74	17.4 [17.0]

^{a} μ^{FET}: maximum field-effect hole mobility. $\mu_{\text{ave}}^{\text{FET}}$: average field-effect hole mobility of more than 5 different devices. ^{b} Y6 was used as the acceptor. ^{c} $J_{\text{SC}}^{\text{EQE}}$: J_{SC} calculated from the EQE spectrum. ^{d} PCE: maximum power conversion efficiency. PCE$_{\text{ave}}$: average power conversion efficiency of more than 10 different cells.

even when heated to 100 °C. In **PNTz1-F** (Fig. 5c), as similar to the case in **PNTz4T**, the absorption spectrum was significantly blue-shifted and became structureless upon heating. In **PTNT1-F** (Fig. 5d), the spectrum changed only slightly with increasing temperature; the change was even less than that in **PTNT2T**. These results also validate that TNT-based polymers have more rigid backbones than NTz-based polymers.

OFET properties

We tested OFET devices with a top-gate/bottom-contact architecture, in which a patterned Au electrode was pretreated with octanethiol, and CYTOP was employed as the dielectric layer.[44] The polymer layer was deposited by spin-coating from a CB

solution and then annealed at 200 °C for 30 min. Fig. 6a and c depict transfer curves and Fig. 6b and d depict output curves of the OFET devices based on these polymers. All polymers exhibited unipolar p-type characteristics with relatively low threshold voltages of around −10 V and high current on and off ratios of ∼10^5. **PTNT2T** showed a field-effect hole mobility (μ^{FET}) of 1.10 cm^2 V^{-1} s^{-1}, which was higher than that of **PNTz4T** (μ^{FET} = 0.81 cm^2 V^{-1} s^{-1}) (Table 3). **PTNT1-F** showed a μ^{FET} of 0.18 cm^2 V^{-1} s^{-1}, which was also higher than its NTz-based counterpart **PNTz1-F** (μ^{FET} = 0.004 cm^2 V^{-1} s^{-1}) (Table 3). Thus, thiophene fusion improved the in-plane charge carrier transport.

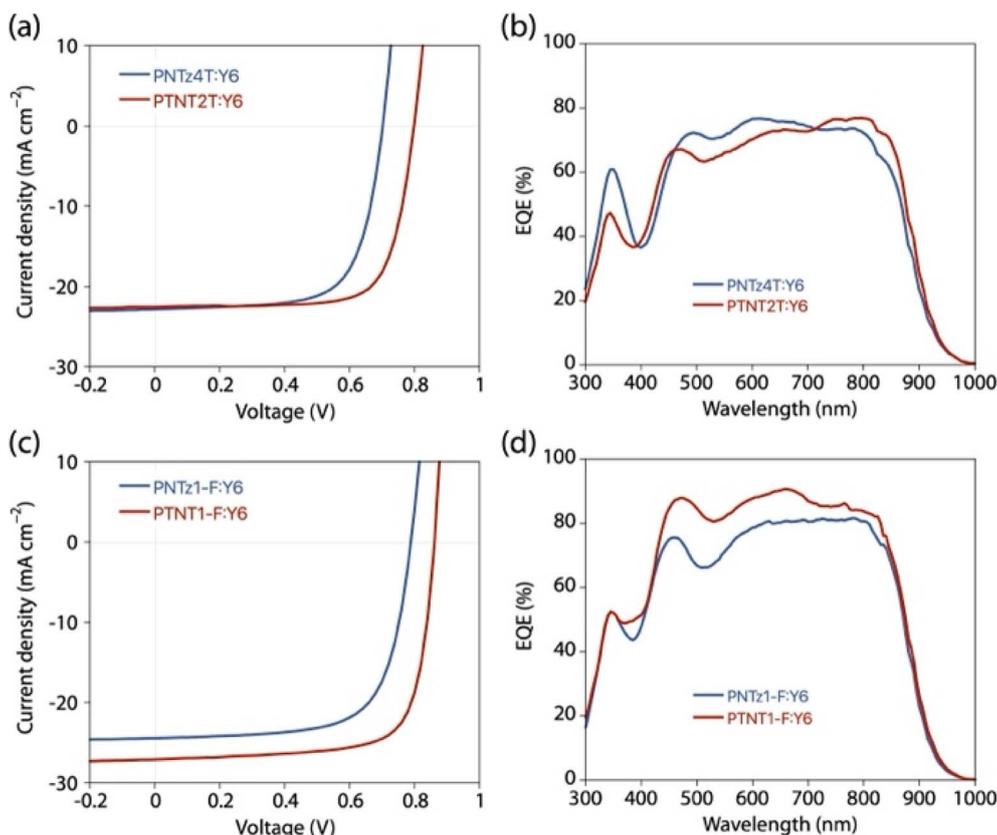**Fig. 7** (a and c) J−V curves and (b and d) EQE spectra of polymer:Y6 cells. (a and b) **PTNT2T** and **PNTz4T** cells and (c and d) **PTNT1-F** and **PNTz1-F** cells.
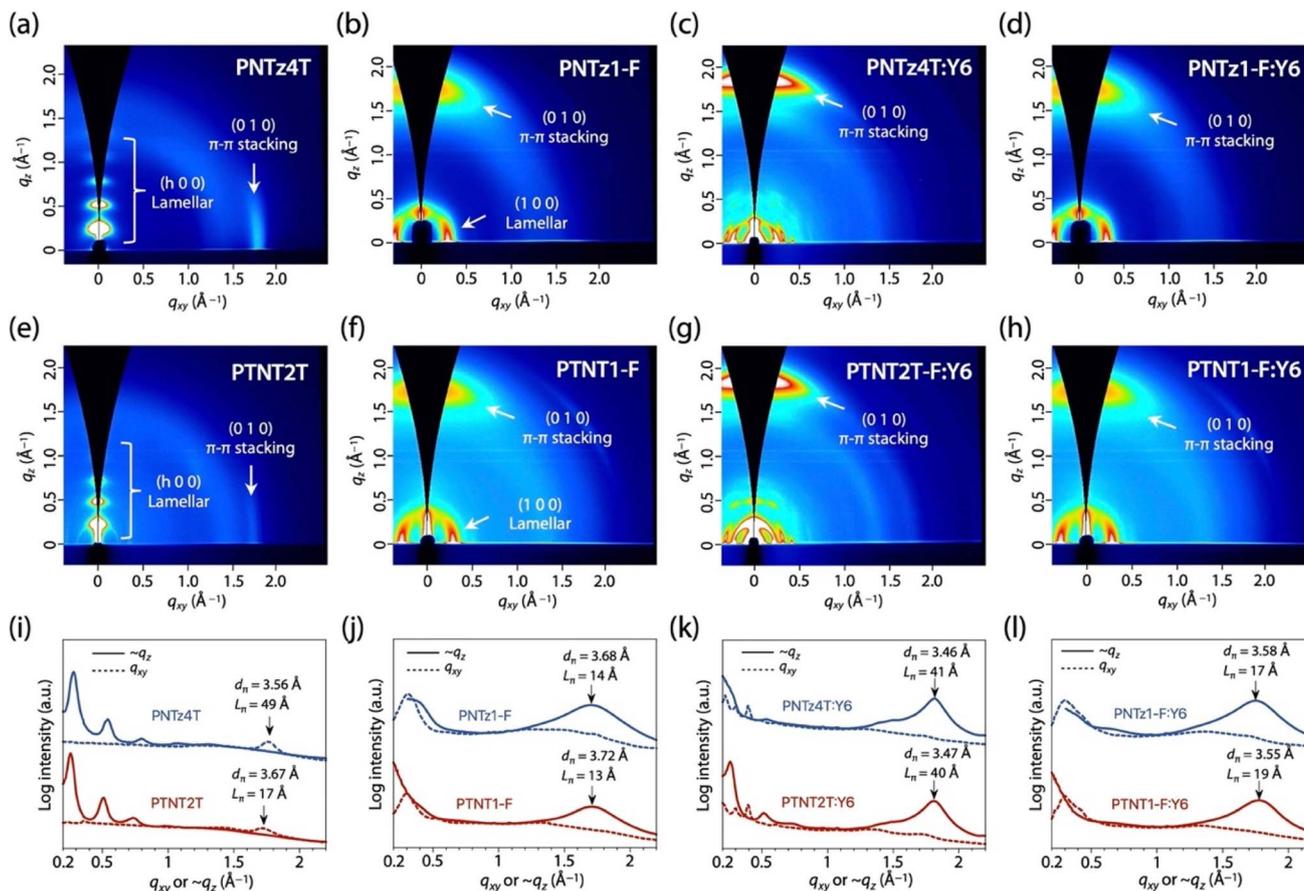
Fig. 8 (a–h) 2D GIXD patterns of polymer neat and blend films. (i–l) Cross-sectional diffraction profiles cut from the 2D GIXD patterns along the quasi-q_z (solid line) and q_{xy} (dotted line) axes. (a, e and i) **PNTz4T** and **PTNT2T**, (b, f and j) **PNTz1-F** and **PTNT1-F**, (c, g and k) **PNTz4T**:Y6 and **PTNT2T**:Y6, and (d, h and l) **PNTz1-F**:Y6 and **PTNT1-F**:Y6.

OPV properties

OPV cells with a conventional structure (ITO/PEDOT:PSS/polymer:Y6/PNDI-F3N-Br/Ag) were fabricated. Fig. 7a and b show the current density–voltage (J–V) curves and the external quantum efficiency (EQE) spectra of the **PTNT2T** and **PNTz4T** cells and Table 3 summarizes the OPV properties. The **PTNT2T** cell exhibited a short-circuit current density (J_{SC}) of 22.5 mA cm^{-2}, which was similar to that of the **PNTz4T** cell (J_{SC} = 22.8 mA cm^{-2}). Both cells exhibited EQEs of approximately 70–80% in the polymer and Y6 absorption regions. The J_{SC} values calculated from the EQE spectra (J_{SC}^{EQE}) were consistent with the J_{SC} values obtained in the J–V measurement (Table 3). Meanwhile, the **PTNT2T** cell exhibited a higher open-circuit voltage (V_{OC}) (V_{OC} = 0.80 V) than the **PNTz4T** cell (V_{OC} = 0.70 V), which can be explained by the lower E_{HOMO} of **PTNT2T** than that of **PNTz4T**. Furthermore, the **PTNT2T** cell provided a higher fill factor (FF) of 0.74 than the **PNTz4T** cell (FF = 0.69). As a result, the **PTNT2T** cell exhibited a PCE of 13.4%, which was higher than that of the **PNTz4T** cell (PCE = 11.1%). Fig. 7c and d show the J–V curves and the EQE spectra of the **PTNT1-F** and **PNTz1-F** cells. The **PTNT1-F** cell exhibited a PCE of 17.4%, which is reasonably high for binary blend OPVs, with a J_{SC} of 27.1 mA

cm^{-2}, a V_{OC} of 0.86 V, and an FF of 0.74 (Table 3). The performance of the **PTNT1-F** cell was markedly higher than those for the **PNTz1-F** cell (PCE = 13.3%, J_{SC} = 24.5 mA cm^{-2}, V_{OC} = 0.79 V, FF = 0.69) (Table 3). The higher J_{SC} was consistent with the higher EQE values in the **PTNT1-F** cell than in the **PNTz1-F** cell, particularly in the 450–650 nm polymer absorption region. The higher V_{OC} in the **PTNT1-F** cell than in the **PNTz1-F** cell is also ascribed to the deeper E_{HOMO} of **PTNT1-F** than that of **PNTz1-F**.

We evaluated out-of-plane hole mobility (μ^{SCLC}) based on the space-charge-limited current (SCLC) model (Fig. S6†). Notably, the μ^{SCLC} of 1.7×10^{-3} cm^2 V^{-1} s^{-1} for **PTNT2T**:Y6 blend film was markedly higher than that for **PNTz4T**:Y6 (μ^{SCLC} = 2.8×10^{-4} cm^2 V^{-1} s^{-1}). Furthermore, the **PTNT1-F**:Y6 blend film exhibited a μ^{SCLC} of 8.0×10^{-4} cm^2 V^{-1} s^{-1}, which was also higher than that for **PNTz1-F**:Y6 (μ^{SCLC} = 1.5×10^{-4} cm^2 V^{-1} s^{-1}). The trend in μ^{SCLC} correlated well with the photovoltaic performance, *e.g.*, J_{SC} and FF.

Polymer order in thin films

We conducted two-dimensional grazing incidence wide-angle X-ray diffraction (2D GIXD) measurements for the polymer neat and blend films on a glass substrate (Fig. 8a, b, e, f, i and j).
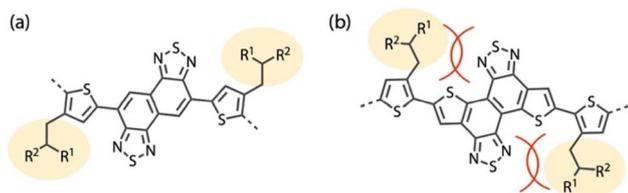
Fig. 9 Schematic illustration of plausible steric hindrance for (a) NTz-based polymers and (b) TNT-based polymers.

PNTz4T and **PTNT2T** neat films showed diffraction corresponding to the (0 1 0) π–π stacking structures and the (h 0 0) lamellar structures along the q_{xy} and $\sim q_z$ axes, respectively, indicating that the backbone orientation was predominantly edge-on for both polymers (Fig. 8a and e). The d-spacing of 3.67 Å (q_{xy} = 1.71 Å^{-1}) for the (0 1 0) π–π stacking structure (d_{π}) of **PTNT2T** was wider than that of **PNTz4T** (d_{π} = 3.56 Å, q_{xy} = 1.76 Å^{-1}) (Fig. 8i). Moreover, the coherence length (L_{π}) calculated using the Scherrer equation for the π–π stacking structure in **PTNT2T** (L_{π} = 17 Å) was significantly shorter than that in **PNTz4T** (49 Å). Thus, although somewhat surprising, the crystallinity of **PTNT2T** diminished compared to that of **PNTz4T** even though the former incorporated a more π-extended core structure than the latter. This was because the alkyl groups were substituted on the thiophene rings at the near side of the TNT moiety in **PTNT2T**. In contrast, the alkyl groups were substituted on the thiophene rings at the far side of the NTz moiety in **PNTz4T** (Fig. 9). As indicated by the computational finding that the TNT–alkylthiophene linkage had a larger dihedral angle than the NTz–alkylthiophene linkage (Fig. S5†), the polymer backbone of **PTNT2T** can be more twisted than that of **PNTz4T**. Meanwhile, **PNTz1-F** and **PTNT1-F** neat films exhibited diffraction corresponding to the (0 1 0) π–π stacking structures and the (1 0 0) lamellar structures along the $\sim q_z$ and q_{xy} axes, respectively, indicating a predominantly face-on orientation (Fig. 8b and f). **PTNT1-F** and **PNTz1-F** showed similar d_{π} values of around 3.7 Å and similar L_{π} values of 13–14 Å (Fig. 8j), which sharply contrast with the trend observed in **PTNT2T** and **PNTz4T**. This is probably because the relatively wide d_{π} and relatively short L_{π} values of **PTNT1-F** and **PNTz1-F** are limited by the intermolecular steric hindrance of the alkylthienyl substituents on the BDT unit. Based on the fact that the TNT-based polymers had lower and/or similar crystallinity compared to the NTz-based polymers, the higher μ^{FET} observed in the TNT-based polymers than those observed in the NTz-based polymers possibly originated from the rigid polymer backbone that could facilitate intramolecular charge carrier transport.

We also conducted 2D GIXD measurements for polymer:Y6 blend films on ITO/PEDOT:PSS substrates to clarify the packing order in the OPV cells (Fig. 8c, d, g, h, k and l). All the blend films showed diffractions corresponding to the (0 1 0) π–π stacking structures in the wide-angle region along the q_z axis, indicating a predominantly face-on orientation that is favorable for charge carrier transport in OPVs. The **PNTz4T**:Y6 and **PTNT2T**:Y6 blend films showed similar d_{π} values shorter than 3.5 Å with the similar L_{π} values of around 40 Å (Fig. 8c, g and k).

In addition, the **PTNT1-F**:Y6 and **PNTz1-F**:Y6 blend films also showed similar π–π stacking diffractions and d_{π} and L_{π} values of around 3.6 Å and 17–19 Å, respectively (Fig. 8d, h and l). These diffractions resulted from the superposition of the π–π stacking diffractions of the polymer and Y6, and the diffraction of Y6 was likely dominant considering the q_z values (Fig. S7 and S8†). Thus, we did not observe significant differences in the packing order between the **PNTz4T**:Y6 and **PTNT2T**:Y6 blend films and that between the **PTNT1-F**:Y6 and **PNTz1-F**:Y6 blend films. In addition, atomic force microscopy indicated no apparent difference in the film morphology of the cells (Fig. S9†). Thus, the high μ^{SCLC} in the TNT-based polymers resulted from the rigid polymer backbone that originated from the π-extended structure of TNT, which plausibly improved the intrachain charge carrier transport.

Conclusion

TNT, a thiophene-fused A building unit for π-conjugated polymers, was designed and synthesized for the first time by a microwave-assisted thienannulation reaction of arylethynylated NTz precursors *via* C–H functionalization. This synthetic methodology can be applied to various electron-deficient rings to afford thiophene-fused A building units. Two polymer systems were synthesized using the TNT building units: **PTNT2T** and **PTNT1-F**. These TNT-based polymers had a shallower E_{LUMO} and a deeper E_{HOMO} than their NTz counterparts (**PNTz4T** and **PNTz1-F**), most likely because of the weaker electron deficiency of TNT than that of NTz. An important structural feature of TNT-based polymers is their rigid backbones due to the π-extended TNT building unit, which are beneficial for charge carrier transport. Indeed, the TNT-based polymers showed higher hole mobilities in both in-plane and out-of-plane directions than the NTz-based polymers. Furthermore, the TNT-based polymers also showed higher photovoltaic performance than the NTz-based polymers. We believe that TNT has great potential as a building unit for high-performance π-conjugated polymers.

Data availability

The data supporting this article have been included as part of the ESI.†

Author contributions

To. M. and S. S. synthesized the monomers and polymers and carried out the UV-vis, CV, DFT calculations, and 2D GIXD experiments. M. H. supported the synthesis of the monomers. Y. S. and H. O. carried out PL measurements. Ts. M. conducted fabrication and measurements of OFET devices. Ts. M., To. M., and S. S. conducted fabrication and measurements of OPV cells. Ts. M. and I. O. prepared the manuscript, and Ts. M., To. M., S. S., and M. H. prepared the ESI.† All authors discussed and commented on the manuscript. Ts. M. and I. O. directed the project.

Conflicts of interest

There are no conflicts to declare.

Acknowledgements

References

1 J. R. Reynolds, B. C. Thompson and T. A. Skotheim, *Handbook of Conducting Polymers*, CRC Press, Boca Raton, 4th edn, 2019.

2 A. F. Paterson, S. Singh, K. J. Fallon, T. Hodsden, Y. Han, B. C. Schroeder, H. Bronstein, M. Heeney, I. McCulloch and T. D. Anthopoulos, *Adv. Mater.*, 2018, **30**, 1801079.

3 J. Chen, J. Yang, Y. Guo and Y. Liu, *Adv. Mater.*, 2022, **34**, e2104325.

4 M. Berggren, X. Crispin, S. Fabiano, M. P. Jonsson, D. T. Simon, E. Stavrinidou, K. Tybrandt and I. Zozoulenko, *Adv. Mater.*, 2019, **31**, e1805813.

5 N. A. Kukhta, A. Marks and C. K. Luscombe, *Chem. Rev.*, 2022, **122**, 4325–4355.

6 M. Riede, D. Spoltore and K. Leo, *Adv. Energy Mater.*, 2021, **11**, 2002653.

7 G. Zhang, F. R. Lin, F. Qi, T. Heumüller, A. Distler, H.-J. Egelhaaf, N. Li, P. C. Y. Chow, C. J. Brabec, A. K.-Y. Jen and H.-L. Yip, *Chem. Rev.*, 2022, **122**, 14180–14274.

8 S. Guan, Y. Li, C. Xu, N. Yin, C. Xu, C. Wang, M. Wang, Y. Xu, Q. Chen, D. Wang, L. Zuo and H. Chen, *Adv. Mater.*, 2024, **36**, e2400342.

9 Y. Jiang, S. Sun, R. Xu, F. Liu, X. Miao, G. Ran, K. Liu, Y. Yi, W. Zhang and X. Zhu, *Nat. Energy*, 2024, **9**, 975–986.

10 F. P. G. de Arquer, A. Armin, P. Meredith and E. H. Sargent, *Nat. Rev. Mater.*, 2017, **2**, 16100.

11 B. Russ, A. Glaudell, J. J. Urban, M. L. Chabinyc and R. A. Segalman, *Nat. Rev. Mater.*, 2016, **1**, 16050.

12 K. Müllen and W. Pisula, *J. Am. Chem. Soc.*, 2015, **137**, 9503–9505.

13 M. Kim, S. U. Ryu, S. A. Park, K. Choi, T. Kim, D. Chung and T. Park, *Adv. Funct. Mater.*, 2019, **10**, 1904545.

14 L. Dou, Y. Liu, Z. Hong, G. Li and Y. Yang, *Chem. Rev.*, 2015, **115**, 12633–12665.

15 M. E. Cinar and T. Ozturk, *Chem. Rev.*, 2015, **115**, 3036–3140.

16 I. McCulloch, M. Heeney, C. Bailey, K. Genevicius, I. MacDonald, M. Shkunov, D. Sparrowe, S. Tierney, R. Wagner, W. Zhang, M. L. Chabinyc, R. J. Kline, M. D. McGehee and M. F. Toney, *Nat. Mater.*, 2006, **5**, 328–333.

17 H. Pan, Y. Li, Y. Wu, P. Liu, B. S. Ong, S. Zhu and G. Xu, *J. Am. Chem. Soc.*, 2007, **129**, 4112–4113.

18 I. Osaka, T. Abe, S. Shinamura and K. Takimiya, *J. Am. Chem. Soc.*, 2011, **133**, 6852–6860.

19 I. Osaka, T. Kakara, N. Takemura, T. Koganezawa and K. Takimiya, *J. Am. Chem. Soc.*, 2013, **135**, 8834–8837.

20 M. Zhang, H. N. Tsao, W. Pisula, C. Yang, A. K. Mishra and K. Müllen, *J. Am. Chem. Soc.*, 2007, **129**, 3472–3473.

21 H. N. Tsao, D. M. Cho, I. Park, M. R. Hansen, A. Mavrinskiy, D. Y. Yoon, R. Graf, W. Pisula, H. W. Spiess and K. Müllen, *J. Am. Chem. Soc.*, 2011, **133**, 2605–2612.

22 W. Zhang, J. Smith, S. E. Watkins, R. Gysel, M. McGehee, A. Salleo, J. Kirkpatrick, S. Ashraf, T. Anthopoulos, M. Heeney and I. McCulloch, *J. Am. Chem. Soc.*, 2010, **132**, 11437–11439.

23 X. Zhang, H. Bronstein, A. J. Kronemeijer, J. Smith, Y. Kim, R. J. Kline, L. J. Richter, T. D. Anthopoulos, H. Sirringhaus, K. Song, M. Heeney, W. Zhang, I. McCulloch and D. M. DeLongchamp, *Nat. Commun.*, 2013, **4**, 2238.

24 D. Venkateshvaran, M. Nikolka, A. Sadhanala, V. Lemaur, M. Zelazny, M. Kepa, M. Hurhangee, A. J. Kronemeijer, V. Pecunia, I. Nasrallah, I. Romanov, K. Broch, I. McCulloch, D. Emin, Y. Olivier, J. Cornil, D. Beljonne and H. Sirringhaus, *Nature*, 2014, **515**, 384–388.

25 K. Takimiya, M. Nakano, M. J. Kang, E. Miyazaki and I. Osaka, *Eur. J. Org Chem.*, 2012, **2013**, 217–227.

26 H. Wang, Q. Shi, Y. Lin, H. Fan, P. Cheng, X. Zhan, Y. Li and D. Zhu, *Macromolecules*, 2011, **44**, 4213–4221.

27 L. Li, F. Meng, M. Zhang, Z. Zhang and D. Zhao, *Angew. Chem., Int. Ed.*, 2022, **61**, e202206311.

28 Y. Fukutomi, M. Nakano, J.-Y. Hu, I. Osaka and K. Takimiya, *J. Am. Chem. Soc.*, 2013, **135**, 11445–11448.

29 M. Saito, I. Osaka, Y. Suda, H. Yoshida and K. Takimiya, *Adv. Mater.*, 2016, **28**, 6921–6925.

30 Y. Wang, Z. Yan, H. Guo, M. A. Uddin, S. Ling, X. Zhou, H. Su, J. Dai, H. Y. Woo and X. Guo, *Angew. Chem., Int. Ed.*, 2017, **56**, 15304–15308.

31 G. W. P. van Pruissen, F. Gholamrezaie, M. M. Wienk and R. A. J. Janssen, *J. Mater. Chem.*, 2012, **22**, 20387–20393.

32 G. Kim, S.-J. Kang, G. K. Dutta, Y.-K. Han, T. J. Shin, Y. Y. Noh and C. Yang, *J. Am. Chem. Soc.*, 2014, **136**, 9477–9483.

33 F. A. Arroyave, C. A. Richard and J. R. Reynolds, *Org. Lett.*, 2012, **14**, 6138–6141.

34 P. Cong, Z. Wang, Y. Geng, Y. Meng, C. Meng, L. Chen, A. Tang and E. Zhou, *Nano Energy*, 2023, **105**, 108017.

35 Q. Liu, Y. Jiang, K. Jin, J. Qin, J. Xu, W. Li, J. Xiong, J. Liu, Z. Xiao, K. Sun, S. Yang, X. Zhang and L. Ding, *Sci. Bull.*, 2020, **65**, 272–275.

36 H. Lu, W. Liu, G. Ran, Z. Liang, H. Li, N. Wei, H. Wu, Z. Ma, Y. Liu, W. Zhang, X. Xu and Z. Bo, *Angew. Chem., Int. Ed.*, 2023, **62**, e202314420.

37 M. Wang, X. Hu, P. Liu, W. Li, X. Gong, F. Huang and Y. Cao, *J. Am. Chem. Soc.*, 2011, **133**, 9638–9641.

38 I. Osaka, M. Shimawaki, H. Mori, I. Doi, E. Miyazaki, T. Koganezawa and K. Takimiya, *J. Am. Chem. Soc.*, 2012, **134**, 3498–3507.

39 I. Osaka and K. Takimiya, *Adv. Mater.*, 2017, **29**, 1605218.

40 V. Vohra, K. Kawashima, T. Kakara, T. Koganezawa, I. Osaka, K. Takimiya and H. Murata, *Nat. Photonics*, 2015, **9**, 403–408.

41 L.-H. Chou, T. Mikie, M. Saito, C.-L. Liu and I. Osaka, *ACS Appl. Mater. Interfaces*, 2022, **14**, 14400–14409.

42 L. Meng, T. Fujikawa, M. Kuwayama, Y. Segawa and K. Itami, *J. Am. Chem. Soc.*, 2016, **138**, 10351–10355.

43 D. Yue and R. C. Larock, *J. Org. Chem.*, 2002, **67**, 1905–1909.

44 A. J. Kronemeijer, V. Pecunia, D. Venkateshvaran, M. Nikolka, A. Sadhanala, J. Moriarty, M. Szumilo and H. Sirringhaus, *Adv. Mater.*, 2014, **26**, 728–733.